SCHOOL OF PHYSICS AND ASTRONOMY

YEAR 4 PROJECT DISSERTATION

SESSION 2021-2022

Name:	Louie Leverett
Student Number:	C1823166
Degree Programme:	MPhys Physics with Astronomy
Project Title:	How bright do hot gaseous haloes around galaxies shine in X-rays?
Supervisor:	Dr. Freeke van de Voort
Primary Assessor:	Prof. Carole Tucker
Second Assessor:	Dr. Paul Clark

Declaration:

I have read and understand Appendix 2 in the Student Handbook: "Some advice on the avoidance of plagiarism".

I hereby declare that the attached report is exclusively my own work, that no part of the work has previously been submitted for assessment (although it may re-use material from the "Summary Report" for **this project** as it is considered part of the same assessment), and that I have not knowingly allowed it to be copied by another person.

The effects of magnetic fields on the properties of gaseous halos around simulated galaxies, including X-ray luminosity.

Louie Leverett

Acknowledgements

I would like to thank my project supervisor Dr. Freeke van de Voort for her excellent teaching and guidance throughout my project. I would also like to thank Andrew Hannington, Andrew Cook, and Hilay Shah for their advice and suggestions throughout my project. Finally, I would like to thank my friends and family for their endless support throughout the year.

Abstract

Cosmological, high-resolution, ‘zoom-in’ simulations similar to that of the Auriga project, are performed with the magneto-hydrodynamical moving mesh code Arepo, to investigate the effects of magnetic fields on the temperature, hydrogen number-density, metallicity and total (0.5-2.0 keV) X-ray luminosity of the gaseous component of simulated halos. It is found that magnetic fields increase the temperature and decrease metallicity of the circumgalactic medium significantly. This might be explained by the decrease in inflow/outflow velocities in the presence of magnetic fields. It is also found that the presence of magnetic fields, only have a small effect on the hydrogen number-density however, the reason for this is not explained in this study. The (0.5-2.0 keV) X-ray luminosity of simulated halos is found to be consistent with observational data from the Chandra X-ray observatory. In particular, it is found to be consistent with the linear log-log relation of X-ray luminosity versus stellar mass normalised by the total star-formation rate of the halos. It is found that the presence of magnetic fields may have little to no effect on the brightness of X-ray emission from the halo gas; however, further study is required to make strong conclusions.

Table of contents

1.0: Introduction

Halos are defined by Wechsler and Tinker 2018 as gravitationally bound regions of matter that have decoupled from the Hubble expansion and collapsed. During collapse, dark matter halts as it reaches the virial equilibrium while baryons, due to their ability to radiate energy, continue to collapse. Baryons reach higher densities where they settle and form discs (van de Voort et al. 2016). The infalling gas shock-heats to the virial temperature of the halo and settles into a hot envelope of gas (Kelly et al. 2021). Where the virial temperature refers to the temperature at which a gravitationally bound system satisfies the virial theorem.

$$M_{vir} = \frac{4}{3}\pi r_{vir}^3 \Delta_c \rho_c \qquad \text{(Equation 1)}$$

The Circumgalactic Medium (CGM) is the gaseous component of dark matter halos (van de Voort et al. 2021) and surrounds discs out to their virial radius, r_{vir}. The virial radius of a halo is usually defined to be where the mean gas density is 200 × critical density of the Universe; see equation 1, where ρ_c is the critical density of the Universe and from convention, Δ_c has a value of 200 (Wechsler and Tinker 2018). The CGM forms a reservoir of gas that fuels star formation and is subject to energetic feedback such as stellar winds, supernovae, and active galactic nuclei (Chadayammuri et al. 2022). “The CGM is potentially the galactic fuel tank, waste dump and recycling centre all at the same time” (Tumlinson et al. 2017). Without the CGM galaxies would starve of new gas and is critical to our understanding of the formation, evolution, and quenching of galaxies (Wijers and Schaye 2021).

The CGM is diffuse and a highly ionised multiphase medium (Choudhury et al. 2019), primarily made up of two phases, i) hot, collisionally ionised gas with temperatures near $T \geq 10^6$ K, ii) cooler phase near $T \leq 10^4$ K (Stinson et al. 2012). Observations of the CGM are challenging however, absorption of light from background galaxies and quasars have revealed cool, (~10^4 K) dense gas clouds in halos (Chadayammuri et al. 2022). Additionally, recent line emission in the X-ray wavelengths from the Chandra X-ray telescope have revealed hot diffuse gas around ~10^6 K (Wang et al. 2016). The CGM reaches these high temperatures through several mechanisms. Cold and metal-poor infalling gas is shock-heated as it enters the halo. And dense metal-rich galactic outflows driven by supernovae, and active galactic nuclei (AGN) provide heating for the warm/hot CGM (Das et al. 2019). Highly ionised metals have provided indirect evidence for a hot phase in the CGM.

The CGM is rich with metals. From theoretical models it probably contains 5-50% of the galactic baryons (Chadayammuri et al. 2022). Tumlinson et al. 2011 revealed that observations of haloes of star-forming galaxies contain an ionised metal mass that likely exceeds that of the galaxies’ interstellar medium. Therefore, it can be concluded that, “The CGM is a major reservoir of highly ionised metals (at z~0)” (Stinson et al. 2012).

Studying emission from the CGM is challenging due to the low surface brightness of the gas (Tumlinson et al. 2017). The emission measure scales with density as n^2 (van de Voort et al. 2016) and the CGM has a low hydrogen gas density. The soft X-ray absorption has so far probed the CGM obtaining total mass and baryon fraction at ~10^6 K (Tumlinson et al. 2017). Hot gas has been detected in the X-ray wavelengths as emission (see Wang et al. 2016). “X-ray emission is bias towards high density, temperature and metallicity” (van de Voort et al. 2016). For lower mass halos (<10^{12} $M_\odot$), X-ray emission is primarily powered by galactic winds i.e., stellar winds, supernovae etc. However, for higher mass halos (>10^{13} $M_\odot$), emission is thought to be powered by gas heated from accretion shock at the virial radius (van de Voort et al. 2016).

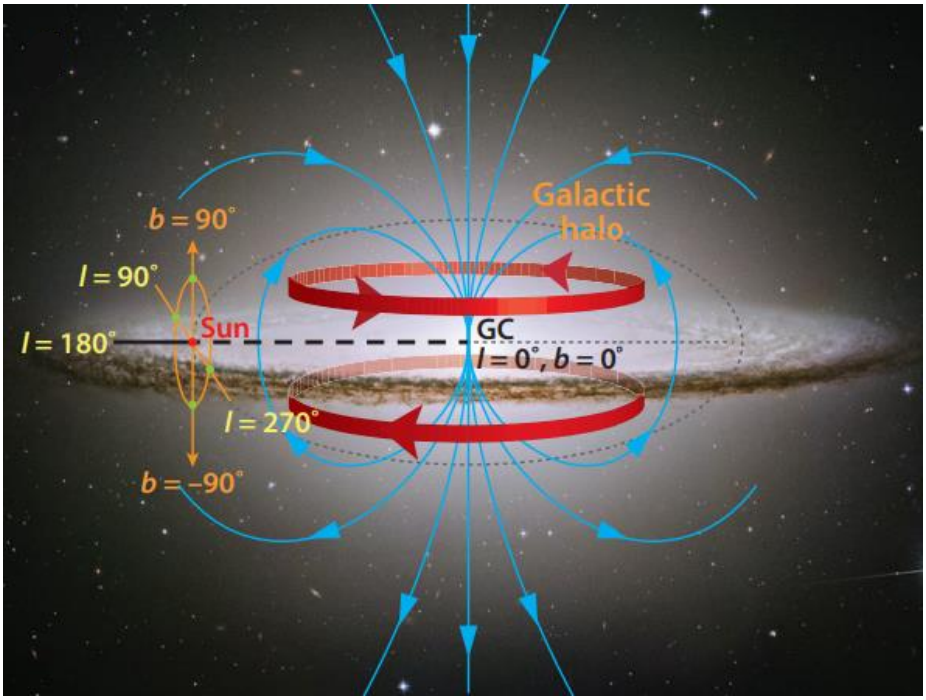

Figure 1: Pictorial representation of idealised magnetic field lines in and among a galactic disc and halo from (Han 2017). The image shows that fields in the halo reverse their directions above and below the galactic plane. Additionally, the image shows fields entering and leaving the galactic poles creating loops within the galactic halo. In reality, the field lines in the CGM are likely more turbulent.

Magnetic fields are omnipresent in galactic discs and their gaseous halos. They are often passive to dynamics (e.g. star formation, galaxy structure, and formation) but play key roles in some stages (Han 2017). For example, magnetic fields can provide additional pressure affecting the evolution of gaseous structures (Han 2017) and they are the main mode of transport of cosmic rays (Giacalone 2013). Additionally, magnetic fields strongly interact with some components of the interstellar medium, e.g., neutral, and ionised gas (Haverkorn and Heesen 2012). The magnetic field strength measured from observations is found to be ~ 9 $\pm$ 3 μG across external galaxy discs (Haverkorn and Heesen 2012). Figure 1, presents a pictorial representation for idealised magnetic field lines, providing a very crude model of magnetic field lines through a galactic disc and gaseous halo. In reality, magnetic field lines may be more turbulent in the CGM due to galactic inflows and outflows.

The origin of galactic magnetic fields has been a long-standing problem in physics (Han 2017). This is due to a lack of observational data as well as a lack of theoretical understanding. Additionally, detecting magnetic fields in low-density environments i.e., galactic halos, is difficult since they are below the detection limit of current instrumentation (Marinacci et al. 2015). However, two proposed models exist in the attempt to explain the origin of magnetic fields. First, seed magnetic fields of cosmological origin that are generated by several processes during inflation, phase transitions and plasma phenomena in the early universe (Widrow et al. 2012). Second, instances of the Biermann battery mechanism (Biermann 1951) are amplified through turbulent dynamo processes, shear flows and/or galactic dynamos as baryons collapse onto dark matter halos. In the second scenario magnetic fields are ejected by galactic winds where AGN contributes to the generation and ejection of fields in the intergalactic medium (Marinacci et al. 2015). It is found from cosmological simulations that magnetic field seeds can be amplified by gravitational collapse, shear flow and turbulence (Dolag et al. 1999). And Dubois and Teyssier 2008 note the importance of cooling processes in the amplification of magnetic fields.

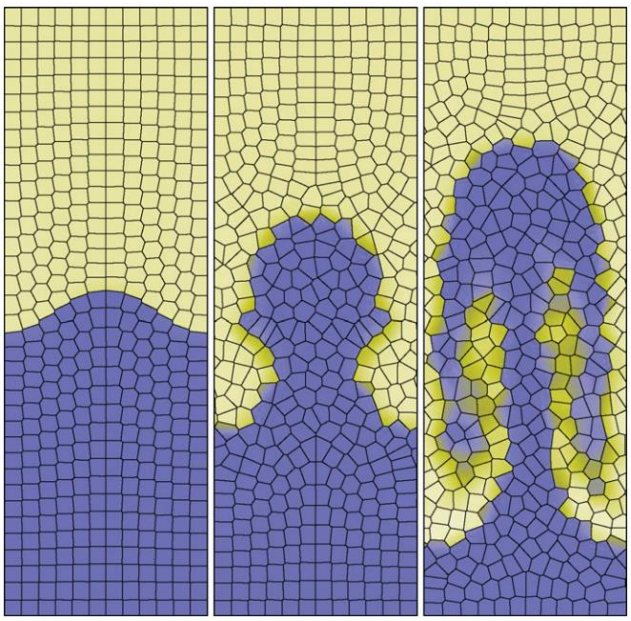

Figure 2: Low resolution Rayleigh-Taylor instability with moving-mesh approach. A denser fluid lies above a less dense fluid, and the hydrostatic equilibrium of the initial state is unstable. The three frames show the time evolution of the moving-mesh at equally spaced time intervals (Springel 2010a).

This project makes use of cosmological, high-resolution, 'zoom-in' simulations, similar to that of the Auriga Project, performed with the magneto-hydrodynamic (MHD) moving mesh code, Arepo (Springel 2010a). 'Zoom-in' refers to the Lagrangian regions (tracked individual regions) belonging to single objects which are sampled with significantly higher resolution than the rest of the cosmological volume. The moving mesh code Arepo, is efficient quasi-Lagrangian code which follows the coupled evolution of dark matter and gas. Arepo makes use of Voronoi mesh code, this mesh allows for a finite-volume discretisation of the Euler equations for magneto-hydrodynamics. Figure 2 demonstrates the evolution of an example moving mesh with time (left to right). It shows a set of discrete mesh-generating points (cells) which move freely and do not overlap.

Magnetic fields are implemented with Arepo, which solves a set of cosmological ideal magnetohydrodynamics equations which are extended to comoving coordinates (see Pakmor and Springel 2013 for a full explanation and derivation of these equations). The halo magnetic field is initialised as a uniform field from the start of the simulation and consistently follows the same ideal MHD equations.

"We demonstrate that our simulations reproduce a wide range of present-day observables, in particular, two-component disc-dominated galaxies with appropriate stellar masses, sizes, rotation curves, star formation rates, and metallicities." (Grand et al. 2017). The Auriga project has proven to be successful for many research areas in galaxy formation and evolution such as reproducing halos (Monachesi et al. 2019), formation of discs (Grand et al. 2017), galactic warps (Gómez et al. 2017), properties of HI discs (Marinacci et al. 2017), disc heating (Grand et al. 2016), satellite quenching (Simpson et al. 2018) and magnetic fields (Pakmor et al. 2017).

This study employs cosmological 'zoom-in' simulations to examine the effects of magnetic fields on the gas properties of simulated halos including, temperature, hydrogen number density, metallicity, and 0.5-2.0 keV X-ray luminosity. Magnetic fields in the Milky Way and other nearby star-forming galaxies are expected to be dynamically important (Pakmor et al. 2017). The MHD code Arepo, grants us the unique ability to consider the effects of magnetic

fields on the properties of the gaseous halo, typically neglected in galaxy formation studies (Pakmor and Springel 2013). This study also examines the consistency between simulated X-ray luminosity and the observational X-ray luminosity of near-by galaxies originally analysed by Li and Wang 2013a.

This report is structured as follows. Section 1.1 will provide the reader with a brief review of past and present research on the CGM, magnetic fields and X-rays, providing a clear understanding on the relevance of this investigation. Section 2 will provide discussion on the methods employed in this project to investigate the halo gas including the properties of the previously simulated halos and a short description of the analysis set-up. Section 3 presents qualitative and quantitative results from this study. Section 3.1 compares and contrasts the differences of gas properties with and without magnetic fields and provides statistical analysis for these differences. Section 3.2 presents analysis on the same effects of magnetic fields with the focus on total 0.5-2.0 keV X-ray luminosity. Measurements of X-ray luminosities are stated for each halo including direct comparison to the latest Chandra observations (Wang et al. 2016). Section 4 is a discussion of these results and leads to conclusions (section 5) on the effects of magnetic fields on halo properties including X-ray emission.

1.1 Literature review

This is an overview of the past and current research of dark matter haloes and their CGM. In particular, how this study fits into the wider research of the gaseous component of dark matter halos. For a current understanding and overview on the nature of the CGM see (Tumlinson et al. 2017).

The CGM has been subject to research since the mid-1950's. Guido Münch observed neutral sodium (Na I) and singly ionised calcium absorption (Ca II) in the spectra for hot stars at high Galactic latitudes (Tumlinson et al. 2017). Lyman Spitzer later published his 1956 paper concluding that Münch's radio noise observations suggest the existence of corona surrounding the Milky Way. "Pressure equilibrium between such a rarefied, high-temperature gas and normal interstellar clouds would account for the existence of such clouds far from the galactic plane and would facilitate the equilibrium of spiral arms in the presence of strong magnetic fields. Observations of radio noise also suggest such a corona." (Spitzer 1956). White and Rees 1978 proposed that the CGM is a crucial part of the galaxy formation process.

By 1995 further evidence for the CGM came about from the results of an imaging and spectroscopic survey of faint galaxies by the Hubble Space Telescope (Lanzetta et al. 1995). It was concluded, "At z<~ 1 most luminous galaxies are surrounded by extended gaseous envelopes of ~160 kpc radius" (Lanzetta et al. 1995). Further absorption surveys were performed and discussed by (Chen et al. 1998). Both studies concluded that galaxy halos contain strong Lyα, C_{IV}, and other metal lines in a "gaseous medium that is richly structured in density, temperature, and ionisation" (Tumlinson et al. 2017). The discovery of quasars had fuelled the observation of absorption spectra which probed many of the observational properties of haloes we know about today.

Since the early-2000s, it has been a combination of observations and models that have driven the current research for the gaseous properties of dark matter halos. In particular, the cosmological simulation projects such as IllustrisTNG, EAGLE Project, and the Auriga Project This report studies the effects of magnetic fields on the CGM of simulated dark matter halos from the Auriga project, while newly measuring the 0.5-2.0 keV X-ray luminosity.

Li and Wang 2013a, established a database of 53 galactic halos with their galactic properties such as the total 0.5-2 keV X-ray luminosity (Lx), star formation rate (SFR) and stellar mass (M*) for highly inclined disc galaxies observed by the Chandra X-ray Observatory. This was followed by further analysis in Li and Wang 2013b, Li et al. 2014 and Wang et al. 2016 which found strong correlations between X-ray luminosity and other halo gas properties such as SFR and stellar mass. In particular, they found strong correlations for Lx and supernova mechanical energy input rate and Lx/SFR versus M*/SFR. This study seeks to examine if the total X-ray luminosity of simulated halos are consistent with the latter corelation additionally quantifying if the simulated and observational data are a match.

Magnetic fields in galaxy halos are largely mysterious. Their effects are not well defined, observationally, or theoretically. However, they are thought to play an essential role in many astrophysical phenomena, for example the physics of accretion on compact objects (Marinacci et al. 2015). This study seeks to understand their effects on gas properties of simulated halos, building upon recent research, for example, van de Voort et al. 2021. Additionally, this study seeks to examine the effects of magnetic fields on the X-ray luminosity of simulated halos. The simulated X-ray emission is compared to the power law scaling relations recently found from the analysis of surveys from Chandra (Wang et al. 2016).

2.0 Method

2.1 Halo simulations

This study makes use of cosmological 'zoom-in' simulations similar to Auriga (Springel 2010b) to examine redshift, z = 0, snapshots of three Milky Way-mass halos. The simulations make use of moving mesh code Arepo (see section 1) which uses a formless Voronoi mesh for the gas and is additionally responsible for MHD. The halos are identified using the SUBFIND algorithm (Springel et al. 2001) and their total masses are measured within the enclosed virial radius, R_{200}, the radius at which the mean over density is 200 times the critical density of the Universe. Each halo is simulated at standard resolution assuming ΛCDM (Lambda cold dark matter) cosmology, with parameters $\Omega_m = 1 - \Omega_\Lambda = 0.307$, $\Omega_\Lambda = 0.693$, $\Omega_b = 0.048$, $h = 0.6777$, $\sigma_8 = 0.8288$, and $n = 0.9611$ at redshift. Every halo is subject to the same Auriga feedback model without AGN, which is thought to be unimportant for star-forming galaxies (van de Voort et al. 2016). The primary source of feedback included in each model is driven by stellar winds and supernovae explosions of massive stars. Every halo is simulated twice, in the presence and absence of magnetic fields. It should be noted that stellar feedback alone does not provide enough energy in the halos for gas temperatures to reach higher than ~10^4 K. It is shock-heated gas and stellar winds that provide the sufficient energy to bring gas temperatures to ~ 10^5-10^6 K. The interstellar medium (ISM) of each halo is described by a subgrid model found at high densities (Grand et al. 2017). Star formation below the resolution limit is governed by the isothermal equation of state if the mesh cells within the ISM have a SFR > 0.

Halo	SFR (Msun yr^{-1})	M_{200} (10^{10} M_{sun})	R_{200} (Mpc)	Metal mass fraction	Magnetic field strength (μG)
Halo 6 (B>0)	2.547	109.725	0.217	0.016	2.155
Halo 6 (B=0)	2.722	102.162	0.212	0.0135	N/A
Halo 12 (B>0)	13.609	117.428	0.222	0.0207	0.964
Halo 12 (B=0)	7.776	108.753	0.216	0.0198	N/A
Halo L8 (B>0)	9.636	92.021	0.205	0.0212	1.106
Halo L8 (B=0)	7.056	83.962	0.198	0.017	N/A

Table 1: Properties of simulated Halos 6, 12, and L8 with and without magnetic fields. The third column presents M_{200}, the mass of the halo measured within R_{200}. The fourth, the metal mass fraction. Finally, the sixth column presents the median magnetic field strength within R_{200}.

Halo 6, 12 and L8 are the Milky Way-mass halos examined in this study and are described in (Grand et al. 2017). Each are similar in properties e.g., star formation rate (SFR), mass, and metallicity; each of these properties are stated in table 1. Halo 6 and 12 are the most similar and are part of the original Auriga suite. Halo L8 however, is part of a suite of slightly lower mass halos (Grand et al. 2019). This selection of simulated halos, although small, present a sample of standard resolution star forming halos. Each halo examined in this study includes satellite discs which affect the results but do not prove to be problematic in the analysis since there are few large, gas rich discs. Additionally, they are easily identified in radial profiles.

2.2 Halo properties

The CGM properties examined in this study are temperature, hydrogen number-density, and metallicity. These properties are analysed in the form of projections, probability density functions (PDFs), radial profiles, and 2D histograms. Additionally, the 0.5-2.0 keV X-ray luminosity is investigated by comparing the correlations found by Wang et al. 2016. Temperature, hydrogen number density, and metallicity are the focus of this study as they might affect the X-ray luminosity of the gas. Each of these halo properties are measured within their viral radius, R_{200}. The ISM cannot be resolved at the resolution seen in these simulations, therefore, the properties examined in this study are measured from the cells where SFR = 0. It should be noted that although the central disc and other satellites do not include their ISM, their gaseous halos still remain.

2.3 Computing and analysing X-ray luminosity

The measurement of X-ray emission from the simulated halos in this study is achieved using the atomic plasma emission database, Pyatomdb. The cooling rate is computed for a range of elements with atomic numbers 1-30 in an energy range of 0.5-2.0 keV. X-rays are measured for each cell individually based on the associated cell temperature and assuming a constant solar metallicity. The emission is originally in the form erg s^{-1} cm^3 which is then converted into luminosity (erg s^{-1}) by considering the mass and density of each gas cell. The total 0.5-2.0 keV X-ray luminosity is computed by summing the emission of every cell within a 200 kpc radius of the galactic centre for halo 12 and L8. Halo 6's total X-ray emission is calculated within only its CGM, 50-170 kpc.

The simulated total X-ray luminosity is compared to observational data. A linear regression algorithm is employed in order to plot a line of 'best-fit' for the observational data as done in (Wang et al. 2016). To evaluate the correlation in the observational data, the Pearson correlation coefficient is employed. The resulting values for Pearson coefficient are found between -1 and +1, meaning a strong negative correlation or a strong positive correlation respectively. In order to quantify a match between the simulated and observational X-ray luminosity data, a two-sample Kolmogorov-Smirnov (KS) test is employed. The KS test quantifies distance between the two underlying continuous distributions of the two independent samples. The KS test assumes a two-sided null hypothesis that the two distributions are identical. The null hypothesis is tested with the associated p-value which indicates the probability of the two data sets coming from the same underlying distribution. A significance value above 0.05, suggests that the null hypothesis can be accepted.

3.0 Results

3.1 Projections

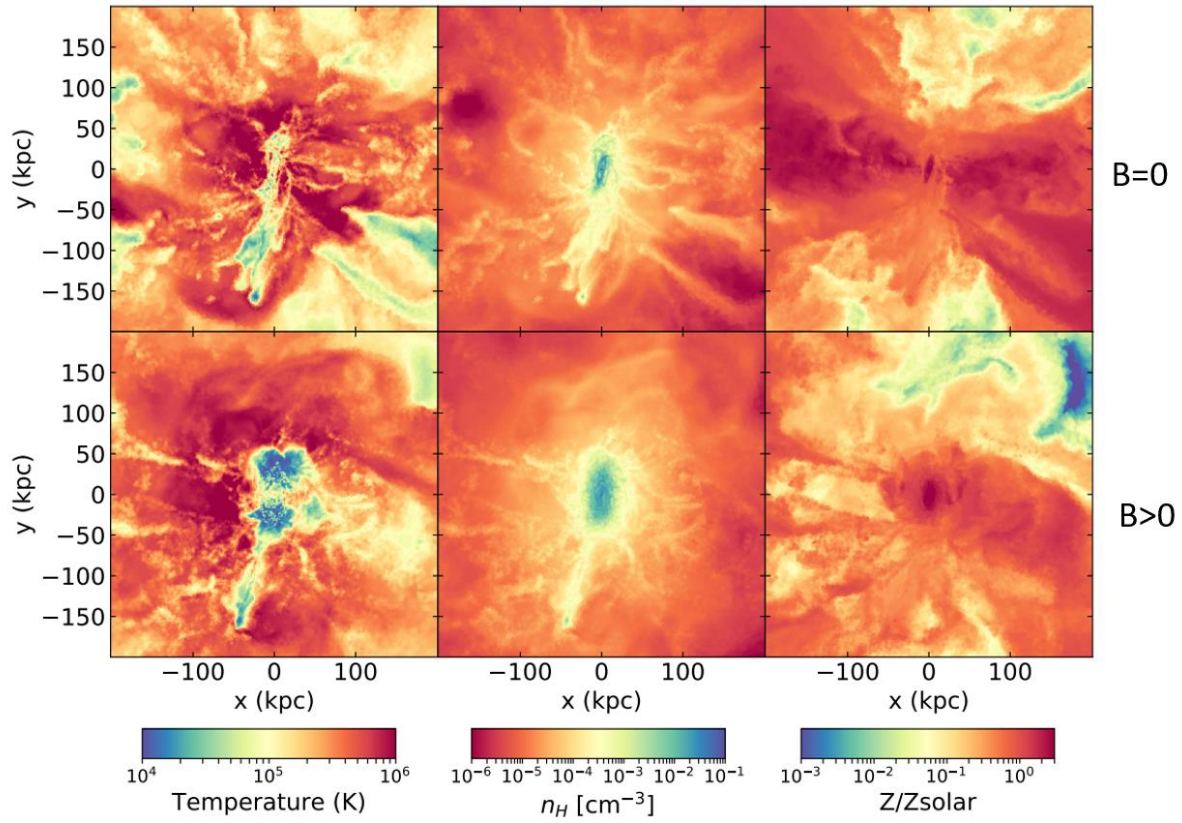

Figure 3: 400 × 400 kpc Projections of Halo 6. Presenting gas Temperature (K) in the first column, hydrogen number density (cm^{-3}) in the second column and metallicity, Z/Zsolar in the third column. The first row shows projections of Halo 6 in the absence of magnetic fields, B = 0. The second row show projections in the presence of magnetic fields, B>0. These projections highlight that magnetic fields have an effect on the properties of the halo gas. In the presence of magnetic fields, the gas seems warmer at radii ≥ 50 kpc, while the disc seems cooler and extended. In the case of hydrogen number-density, it seems there is little change other than an extended higher density disc. In the presence of magnetic fields there seems to be a reduction in the abundance of metals in the CGM (≥ 50 kpc) while in the absence of magnetic fields, there seems to be a greater abundance of metals in the CGM. In both cases, the central disc seems to retain a high metallicity.

Projections of halo 6 are plotted in figure 3 within a 400 x 400 kpc box and a 50 kpc line-of-sight centred on the central halo disc. Each column is plotted with a different colour mesh to distinguish between different gas properties, the first, second and third columns, represent temperature, hydrogen number-density, and metallicity respectively. The first and second row differ by the absence and presence of magnetic fields in that order. Figure 3 is representative for the projections of the other simulated halos 12 and L8 which can be found in the appendix, figures 1 and 2.

Each halo sees a temperature range of 10^4-10^6 (K), a hydrogen number density range of 10^{-6} –10^{-1} (cm^{-3}) and a metallicity, Z/Zsolar of 10^{-3}-10^0. In the case of gas temperature, in the presence of magnetic fields the CGM gas seems warmer overall with temperatures closer ~10^6 K. While the central disc seems to be extended and cooler with temperatures ~10^4 K. For the hydrogen number-density of the halo, it seems that the presence/absence of magnetic fields show little impact. In the presence of magnetic fields, the disc is again seen to be extended with dense gas while the rest of the gas in the CGM seems fairly diffuse. Additionally, the absence of magnetic fields in the hydrogen number-density projections seem to highlight

the existence of some gas filaments with a density of ~10^{-3}-10^{-4} cm^{-3}. Magnetic fields arguably have a greater effect on the abundance of metals throughout the CGM. In the presence of magnetic fields the CGM seems more quenched of metals, and they seem to be retained in greater amounts within the central disc. However, in the absence of magnetic fields the CGM seems to contain a higher metallicity overall. Additionally, in the absence of magnetic fields, there seems to be some defined high metallicity outflows of gas. In either case, the central disc sees the highest abundance of metals.

In the presence of magnetic fields, the CGM seems to be warmer, and there is a lower abundance of metals. There also seems to be little difference in the number-density of hydrogen in the presence/absence of magnetic fields. It seems that turning magnetic fields off allows hot, metal-rich gas to escape the grasp of the central disc and to higher radii. Perhaps then the filaments/outflows seen in the hydrogen and metallicity projections are indeed outflows. The results found here are consistent with Halo 12 and Halo L8.

3.2 Probability Density Functions

Probability density functions (PDFs) for CGM temperature, hydrogen number-density, and metallicity are seen in figures 4-9. PDFs are measured within a radial shell of thickness specific to each halo depending on the size of the disc and position of satellites, only probing the CGM and avoiding the halo discs. Additionally, PDFs are measured for halo cells where SFR = 0. The shell thicknesses for Halo 6, 12, and L8 are measured between 50-170 kpc, 100-200 kpc, and 80-190 kpc respectively, approximately each having a shell thickness of ~100 kpc. So, PDFs are plotted focusing only on the gas in the CGM, quantifying the effects of magnetic fields on the gas properties excluding the ISM and gas of the central and satellite discs. PDFs for the full halo radii i.e., 0-200 kpc, of each simulated halo are seen in the Appendix, figures 3-8.

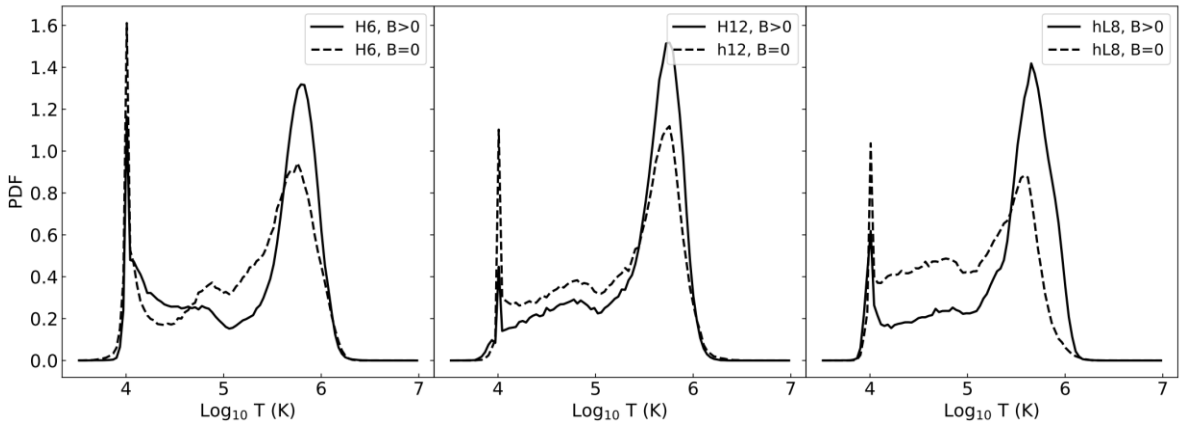

Figure 4: Probability density functions (PDFs) for CGM gas temperature of halos 6, 12 and L8. Each subplot presents a PDF for magnetic fields on and off, indicated by a solid and dashed black line respectively. In the presence of magnetic fields (solid line) there is a greater probability of hot gas ~10^6 K than cool gas. While in the absence of magnetic fields, the probabilities of both hot and cold gas are roughly the same.

Figure 4 presents probability density functions (PDFs) for CGM gas temperatures of halo 6, 12 and L8. The presence and absence of magnetic fields is indicated by a solid and dashed line respectively. The PDFs for each halo show a temperature range of 10^4-10^6 K. For all three halos, in the presence of magnetic fields there is a greater probability of hot gas ~10^6 K than cool gas ~10^4 and a reduction in the probability of the intermediate gas temperatures ~10^5 K. Therefore, the presence of magnetic fields creates greater divisions in the gas temperatures. While in the absence of magnetic fields, the probabilities of finding hot or cool gas is roughly the same.

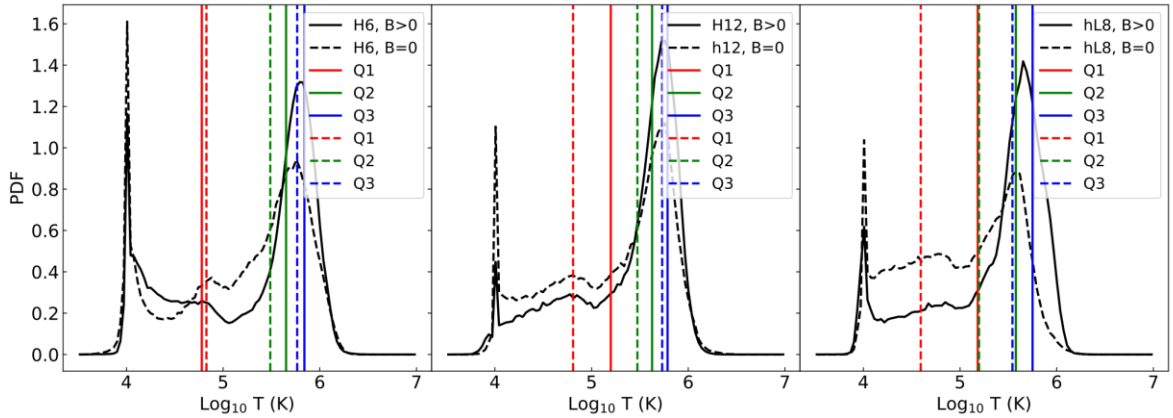

Figure 5: Probability density functions (PDFs) for CGM gas temperature of halos 6, 12 and L8. Each subplot presents a PDF for magnetic fields on and off, indicated by a solid and dashed black line respectively. The vertical lines, in red, green, and blue are the 1st, 2nd and 3rd quartiles each with their respective solid and dashed lines to signify the presence/absence of magnetic fields.

Figure 5 presents PDFs for CGM gas temperatures of halo 6, 12 and L8. The presence and absence of magnetic fields is indicated by a solid and dashed lines respectively. Figure 5 is much like figure 4 however, it additionally includes the 25th, 50th and 75th percentiles seen in the red, green, and blue vertical lines. This helps to quantify the impact of magnetic fields on the amount of gas found at different gas temperatures. It is found from the 75th percentile (Q3) that in the presence and absence of magnetic fields that most of the gas is found below 10^6 K, the hotter regime of gas temperature. Overall, the percentiles indicate that in the presence of magnetic fields the percentile lines are pushed to warmer temperatures.

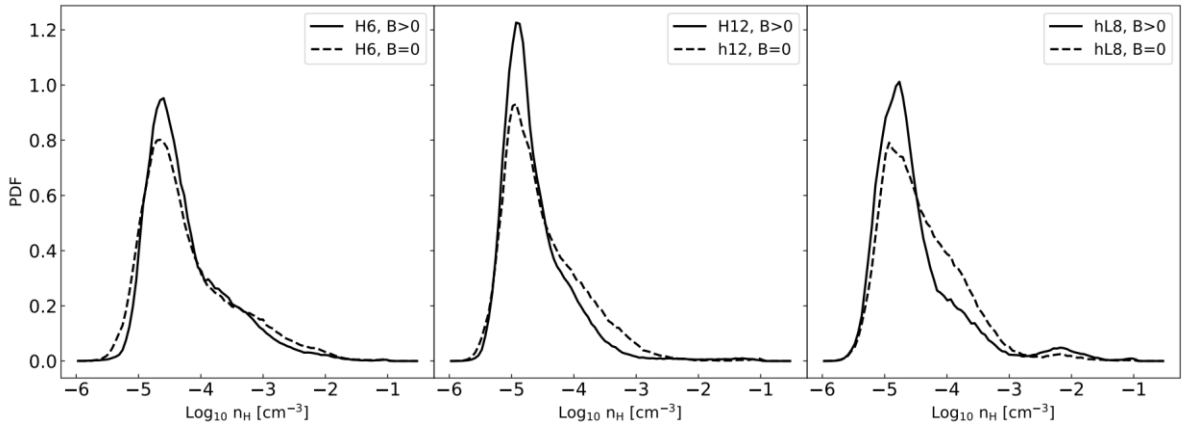

Figure 6: Probability density functions (PDFs) for hydrogen number-density in the CGM of halos 6, 12 and L8. Each subplot presents a PDF for magnetic fields on and off, indicated by a solid and dashed black line respectively. Both distributions for the presence/absence of magnetic fields have approximately the same shape and peak around the same gas densities.

Figure 6 presents PDFs for the hydrogen number-density for the gas of Halo 6, 12 and L8 with and without magnetic fields, indicated by the solid and dashed lines respectively. In all three halos there is a number-density range of 10^{-6}–10^{-1} cm^{-3}, matching the range seen in projections. The PDFs for each halo, both in the presence and absence of magnetic fields, follow roughly the same distribution shape and both peak between 10^{-5} and 10^{-4} cm^{-3}. In the presence of magnetic fields there is a slightly higher probability for the number-density in the range 10^{-5}-10^{-4} cm^{-3}, though the difference in probability is small. Overall, the small difference in height of the peaks indicates that magnetic fields have a small effect on the hydrogen number-density.

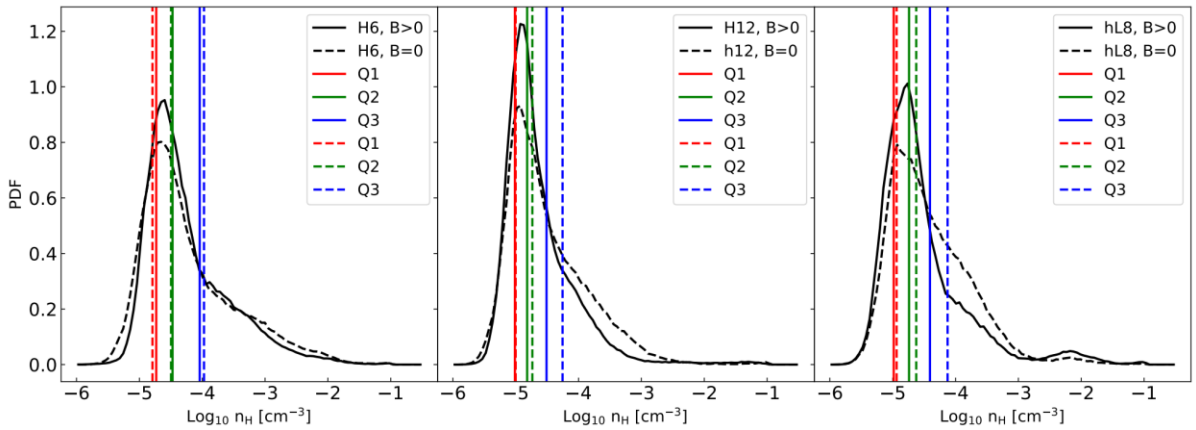

Figure 7: Probability density functions (PDFs) for Hydrogen number-density in the CGM of halos 6, 12 and L8. Each subplot presents a PDF for magnetic fields on and off, indicated by a solid and dashed black line respectively. The vertical lines, in red, green, and blue are the 1st, 2nd and 3rd quartiles each with their respective solid and dashed lines to signify the presence/absence of magnetic fields.

Figure 7 presents the same PDFs seen in figure 6 with the addition of the 25th, 50th and 75th percentiles, indicated by the vertical red, green and blue solid and dashed lines respectively. The solid and dashed lines indicate the presence and absence of magnetic fields. Figure 7 further presents evidence that the effects of magnetic fields are small on hydrogen number-density, indicated by the small change in the positioning of the percentile lines. In the presence of magnetic fields there is a small decrease in the positioning of the percentiles to small number-densities, however, this change is small.

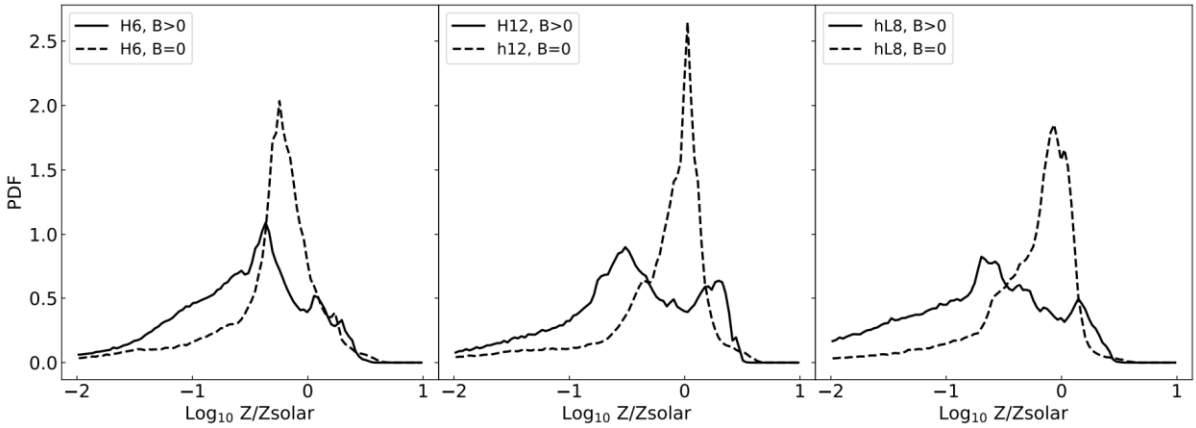

Figure 8: Probability density functions (PDFs) for metallicity in the CGM of halos 6, 12 and L8. Each subplot presents a PDF for magnetic fields on and off, indicated by a solid and dashed black line respectively.

Figure 8 presents the PDFs for the metallicity in the CGM of halos 6, 12 and L8 with and without magnetic fields, indicated by the solid and dashed lines respectively. In the presence of magnetic fields, the probability for metallicities between 10^{-2} and 10^{0} is generally higher, however, it does not peak as high at 10^{0} when in the absence of magnetic fields. Therefore, in the presence of magnetic fields, there is a greater variation in the metallicities. Overall, both distributions suggest that all three simulated halos show high values of metallicity, supporting evidence that the CGM is metal rich.

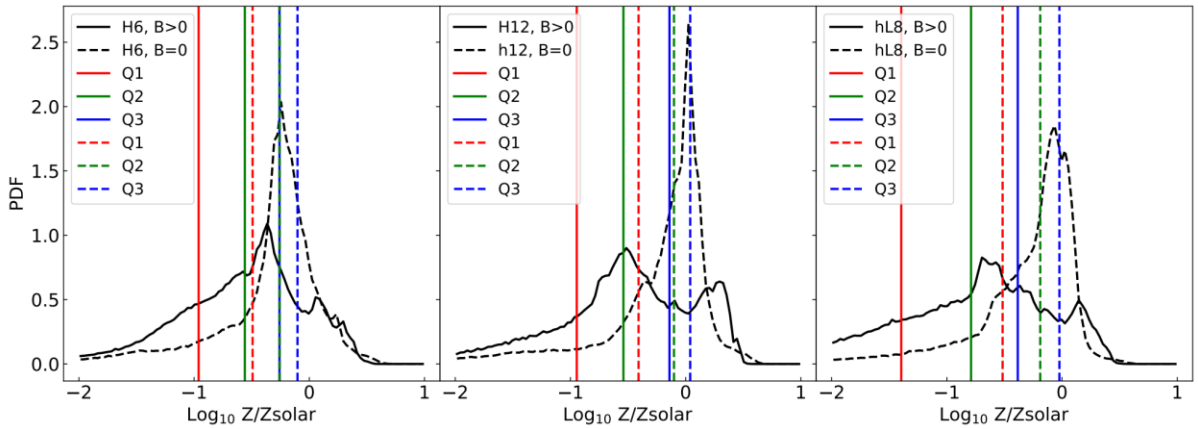

Figure 9: Probability density functions (PDFs) for metallicity in the CGM of halos 6, 12 and L8. Each subplot presents a PDF for magnetic fields on and off, indicated by a solid and dashed black line respectively. The vertical lines, in red, green, and blue are the 1st, 2nd and 3rd quartiles each with their respective solid and dashed lines to signify the presence/absence of magnetic fields.

Figure 9 presents PDFs for metallicity in the same form as figure 8 but with the addition of the 25th, 50th and 75th percentiles indicated by the vertical red, green and blue solid and dashed lines respectively. The solid and dashed lines indicate the presence and absence of magnetic fields. It is immediately apparent that the presence of magnetic fields has an effect on percentile lines. In the presence of magnetic fields, the metallicity is lower, this is most apparent in the 25th percentile line, Q1, where 25% of the data is found at a metallicity ~10^{-1} cm^{-3}. This indicates that in the presence of magnetic fields, the abundance of lower metallicity gas becomes more important. However, most of the gas is found at a metallicity ~10^{0} indicated by the 75th percentile line, Q3.

3.3 Radial profiles

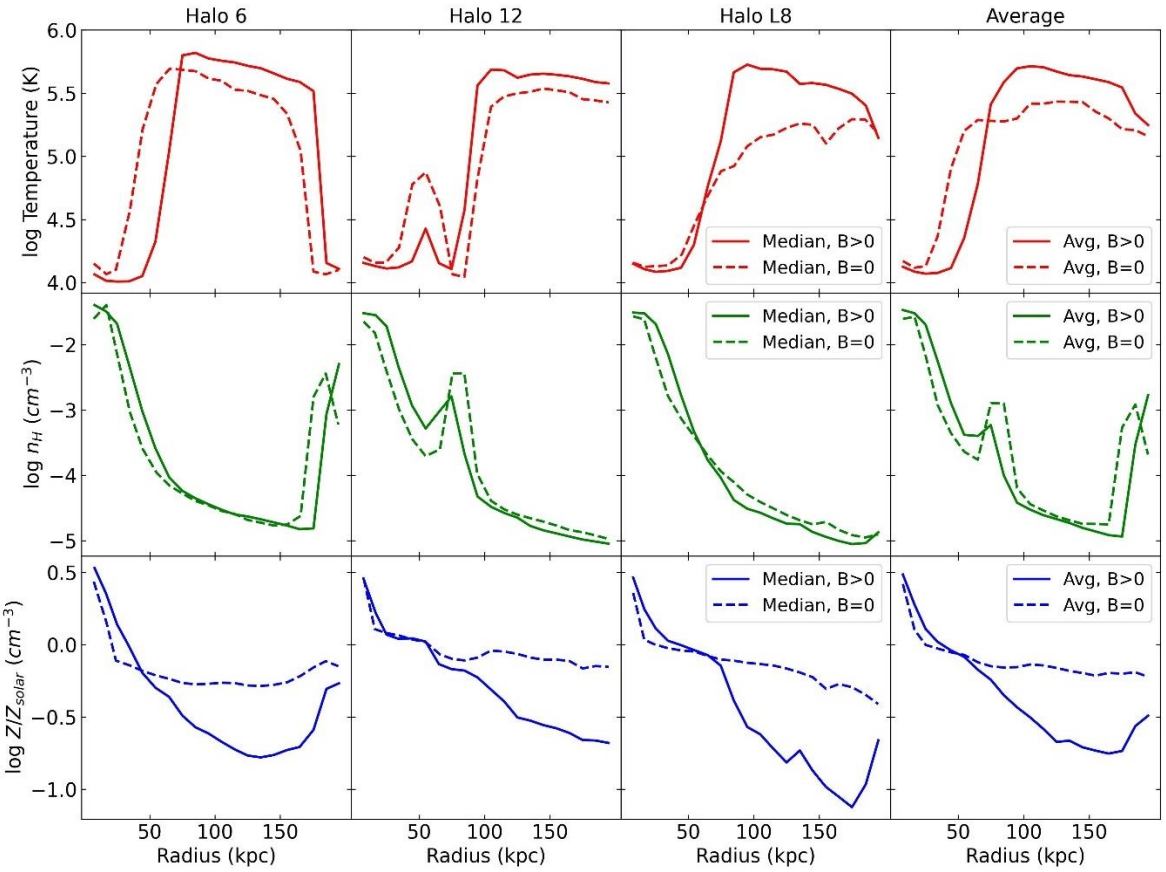

Figure 10: Radial profiles of each halo (distinguished by each column), for the median temperature (K), hydrogen number density, n_H (cm^{-3}), and metallicity, Z/Z_{solar} (distinguished by each row) out to the halo virial radius, R_{200c} ~ 200 kpc. The median is calculated using 10 kpc bins out to 200 kpc, starting at 0-10 kpc. Halos with/without magnetic fields are presented by solid and dashed lines respectively. The radial profiles include the central disc and satellites usually seen by sharp rises or dips. The last column shows the mean of these properties for all three halos. In the presence of magnetic fields, the CGM is warmer, and the hydrogen-number density is more diffuse (however, the difference is small). Additionally, the abundance of metals is lower in the presence of magnetic fields.

Figure 10 presents radial profiles for each halo (distinguished by each column) for the median temperature (K), hydrogen number density (cm^{-3}), and metallicity, Z/Z_{solar} out to 200 kpc. Each profile presents the median for when magnetic fields are on, B>0 and magnetic fields off, B=0 represented by the solid and dashed line respectively. Radial profiles are calculated using multiple identically thick shells of 10 kpc measured from the galactic centre out to 200 kpc. For each shell, the median is calculated for the given gas property and its radius. The radial profiles are calculated so that they include the central disc and satellites, these affect the values of the properties usually seen in a sharp increase or decrease in the radial profile. The final column takes the mean of each property for all three halos and plots the associated radial profile. Each halo has a disc roughly between 0-50 kpc. Therefore, the effect of magnetic fields is primarily studied beyond 50 kpc. Within the CGM, all three halo properties seem to decrease with radius (excluding subhalos).

In the presence of magnetic fields, the median CGM temperature is higher than in the absence of magnetic fields. This is the case for all three halos. This is also the case for the average temperature profile. At smaller radii, 0-50 kpc the gas temperature is initially hotter in the absence of magnetic fields. However, beyond 50 kpc the gas temperature for the presence of the magnetic fields dominates for the remainder of the radii. Both in the presence and absence

of magnetic fields, the gas temperature starts to drop off at larger radii ~150 kpc probably due to a satellite disc.

The hydrogen number-density seems to be mostly indifferent across the 200 kpc radius in both the presence and absence of magnetic fields across all three halos. There is a slightly higher number density in the presence of magnetic fields retained within the central discs (~0-50 kpc) and within the satellite discs, however beyond this radii i.e., within the CGM, the density is low ~10^{-4}–10^{-5} cm^{-3} for both in the presence and absence of magnetic fields. From the average radial profiles for the temperature and hydrogen number-density (both with and without magnetic fields), the CGM (50-170 kpc) is at ~$10^{5\text{ - }6}$ K and ~10^{-5} - 10^{-4} cm^{-3}, supporting the idea of a diffuse and warm CGM.

Across all three halos, the presence of magnetic fields seems to decrease the abundance of metals more steeply with radius while in the absence of magnetic fields the metallicity remains roughly constant. Since metallicity is plotted in log, the decrease in metallicity with radius is likely exponential. From the average radial profile, the presence of magnetic fields seems to decrease the metallicity by ~ 0.5 dex. The metallicity seems to pick up again once the measurements meet a satellite disc. Therefore, in the presence of magnetic fields, the CGM metallicity is lower than when there is an absence of magnetic fields.

3.3.1 Quantifying the difference in radial profiles

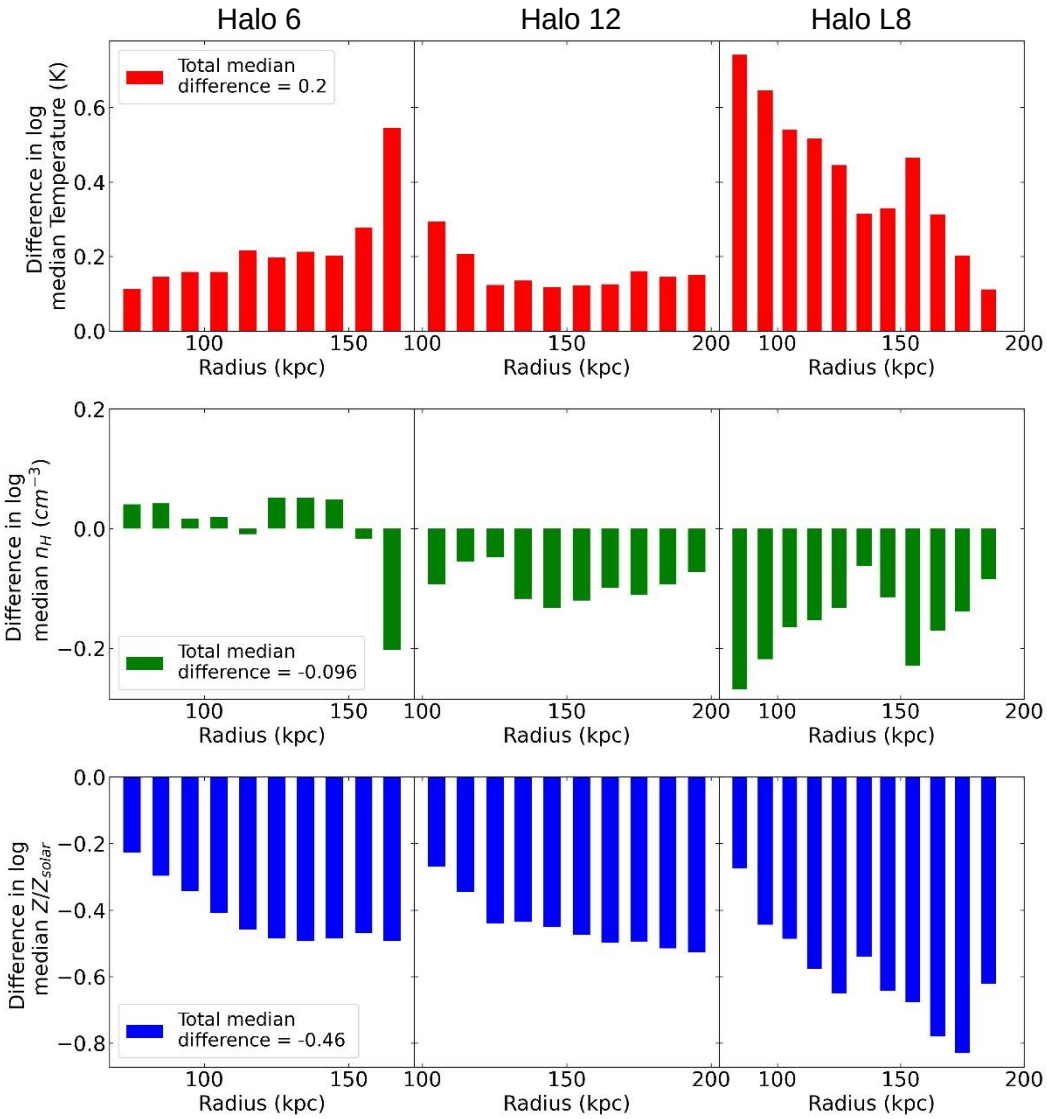

Figure 11: Radial profiles for the difference between the log median temperature, hydrogen number-density, and metallicity, (distinguished by the first, second and third row) in the presence and absence of magnetic fields. The difference is calculated by subtracting the median of B=0 from the median of B>0 and specifically exclude the gas from the halo discs. The first, second and third columns distinguish halo 6, 12, and L8 respectively. The total median difference for each gas property in dex is seen in the figure legend at the start of each row. A positive value means that the property is higher in value in the presence of magnetic fields. A negative value means that the property is higher in value in the absence of magnetic fields.

Figure 11 quantifies the difference in radial profiles for the presence of magnetic fields and the radial profiles in the absence of magnetic fields seen in figure 10. This difference is plotted for the temperature, hydrogen number-density, and metallicity for each simulated halo (indicated by each column). The difference is calculated between the medians of the radial profiles by subtracting the median B=0 radial profile from the median B>0 radial profile. Additionally, the differences are calculated within a specific radii in order to exclude the gas from the halo discs. These radii are as follows, 50-170 kpc, 100-200 kpc, and 80-190 kpc. These radii were chosen to manually remove the disc gas properties seen as peaks and dips in figure 10. The total median difference for each property in the CGM is found in the first column of each row. A positive value means that the property has a higher value in the presence of magnetic fields, while a negative value means that the property has a higher value in the absence of magnetic

fields. Figure 11 allows a visual representation of the direct difference in the median properties across the CGM of each simulated halo.

In the presence of magnetic fields the CGM is warmer by a median average of 0.2 dex across all three simulated halos. Since this difference is positive, this supports the idea that the CGM is warmer in the presence of magnetic fields. The greatest difference is seen in halo L8 which has a median difference of 0.45 dex. In the presence of magnetic fields the hydrogen number-density is smaller than in the absence of magnetic fields. However, the difference is small with a difference of only 0.096 dex. This indicates that the effect of magnetic fields is small on the hydrogen number-density within the CGM. In the presence of magnetic fields, there is a smaller metallicity than in the absence of magnetic fields, i.e., in the absence of magnetic fields there is a greater abundance of metals in the CGM. There is a median average difference of 0.46, the largest difference of all three gas properties studied. This suggests that magnetic fields might have the greatest effect on the metals in the CGM.

3.3.2 Radial profiles for magnetic field strength

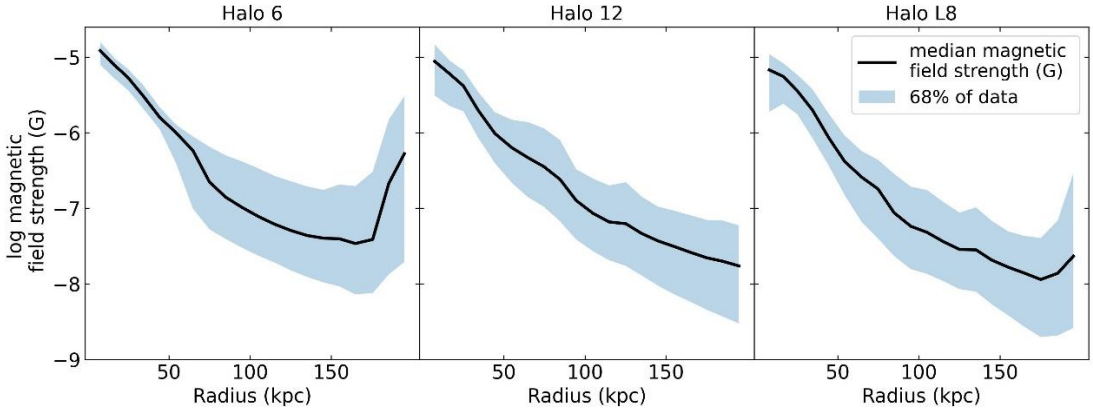

Figure 12: The log magnetic field strength (Gauss) versus halo radius (kpc) between 0-200 kpc, (indicated by the black solid line) including the 16th and 84th percentiles highlighted by the light blue regions, representing a 68% scatter of the magnetic field data, for Halo 6, 12, and L8.

Figure 12 presents the log median magnetic field strength versus radius for halo 6, 12, and L8 between 0-200 kpc, centred on the central disc (excluding regions of star formation). Figure 12 includes a 68% scatter calculated with the 16th and 84th percentile to show that most of the data follows the same trend that the median magnetic field strength (Gauss) decreases with radius. Since the magnetic field strength is in log, and the decline of the field strength is roughly a straight line, the decline of the magnetic field strength with radius is likely exponential. The magnetic field strength starts at around 10^{-5} G at the central disc then decreases to roughly 10^{-8} G around the virial radius, R_{200}, a decrease of ~3 dex. This is the case for all three simulated halos. The slight increase ~1 dex at 200 kpc for halo 6 and L8, is likely due to satellites. Figure 12 may help explain the more rapid decline of temperature, and metallicity seen in the radial profiles when in the presence of magnetic fields (see figure 10).

3.4 2D Histograms

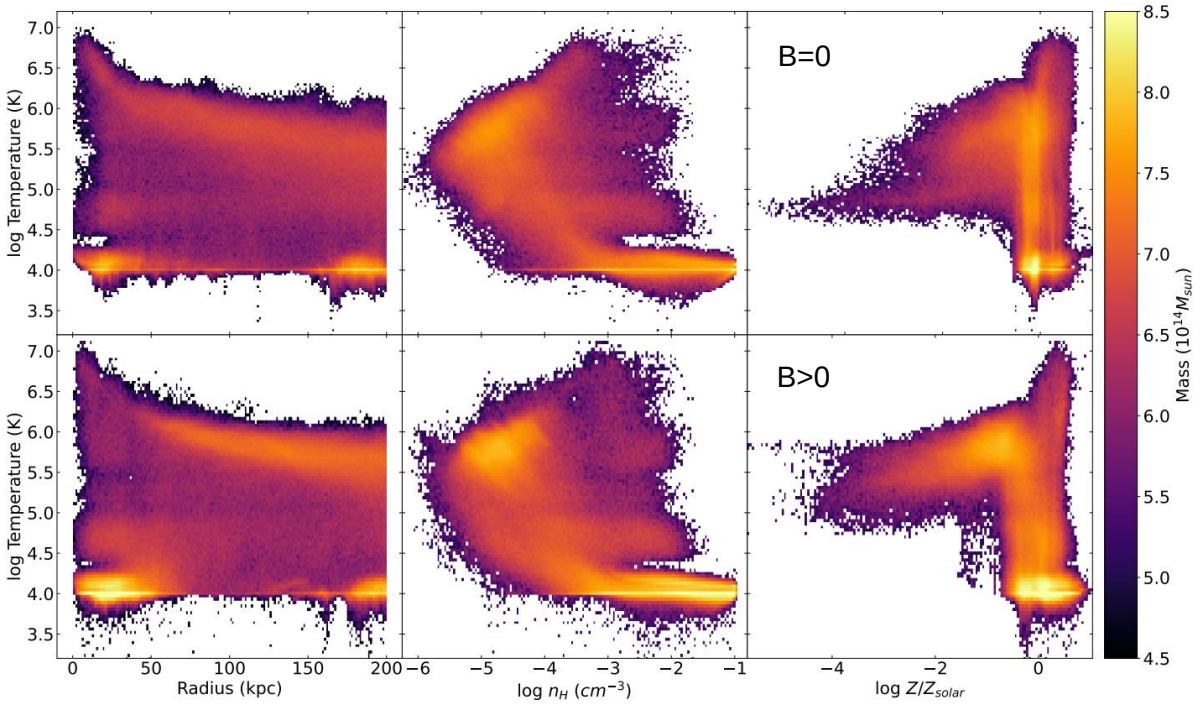

Figure 13: 2D histograms for temperature versus radius, hydrogen number-density, and metallicity, all weighted by cell mass for Halo 6. Each property is represented by each column left to right respectively. The first row presents the histograms without magnetic fields while the second row presents the histograms with magnetic fields. The colour gradient represents the mass of the gas, indicated by the colour bar on the far right of the figure. The histograms provide further evidence that in the presence of magnetic fields, the CGM is warmer, a slight increase in number-density of hydrogen, yet is mostly indifferent, and finally, is lower in the abundance of metals.

Figure 13 presents 2D histograms for temperature (K) versus radius (kpc), hydrogen number-density (cm^{-3}) and metallicity, weighted by cell mass for halo 6. Each gas property is represented by the first, second, and third column respectively. The absence of magnetic fields is seen in the first row while the presence of magnetic fields is seen in the second row. The histograms are calculated by recording all the cells within the 200 kpc with their associated properties including their radii. The data is then evenly distributed into bins of size 150. The histograms are weighted by cell mass which is represented as a colour gradient indicated by the colour bar on the far right of figure 13. Each histogram includes gas for the central disc and satellites which are identified and discussed in the following sections. The following results are consistent with all three simulated halos.

Within the disc, 0-50 kpc, the temperature range is large ~10^4-10^7 K. From the colour gradient, the disc mostly contains cool gas but also contains the hottest gas found in the halo ~10^7 K (however, only a small fraction of the gas is found at this temperature). Moving beyond 50 kpc, the CGM contains mostly hot gas ~10^6 K, seen by the mass weighting but does however, still contain cool gas ~10^4 K. Beyond 170 kpc, the temperature becomes more greatly weighted by cooler gas, indicating the location of a halo satellite. These trends are found in histograms for both the presence and absence of magnetic fields. However, in the presence of magnetic fields the CGM (> 50 kpc) seems to hold most of its mass in the hot gas temperatures ~10^6 K, further supporting evidence of a hot CGM.

In the second column of figure 13, temperature versus hydrogen number-density, it is apparent that the warmer gas ~10^6 K is found at low number-densities ~10^{-5} cm^{-3}, while cooler gas is found at higher number-densities. Additionally, there is a notable amount of low-density cool

gas, seen by the mass weighting. In the presence of magnetic fields, these same trends are found but with higher amounts of gas mass, however, the difference is small.

The third column of figure 13, temperature versus metallicity, shows there is a higher amount of metals found at low gas temperatures. However, high metal abundances are found across the full temperature range, 10^4-10^7 K. The lowest temperatures contain the most amount of metals, probably highlighting the properties of the halo discs. In the presence of magnetic fields, more metals are found in higher gas temperatures but are found at slightly lower metallicities (consistent with PDFs figures 4-9). Additionally, there is a higher amount of cool, high metallicity gas, again probably due to halo discs.

3.5 X-ray Luminosity (0.5-2 keV)

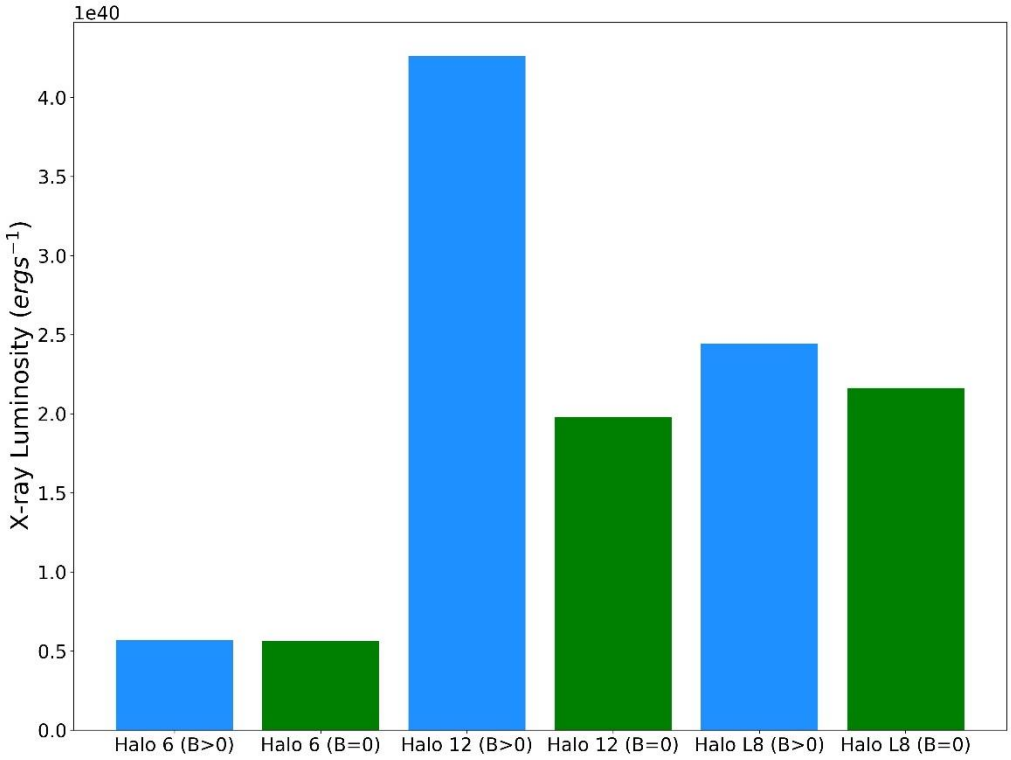

Figure 14: Bar graph for the total (0.5-2.0 keV) X-ray luminosity of each simulated halo (6, 12, and L8) with and without magnetic fields, indicated by the blue and green bars respectively. The total luminosity was measured between 50 and 170 kpc for halo 6 and between 0-200 kpc for halo 12 and L8.

The effects of magnetic fields on the total (0.5-2 keV) X-ray luminosity is seen in figure 14. The X-ray luminosity is measured between 50-170 kpc for halo 6, in order to exclude halo discs. However, between 0-200 kpc for halos 12 and L8. Each halo has a luminosity in the order of 10^{40} erg s^{-1}. The effects of magnetic fields on halo 6 and 12 are small, whereas the effect for halo 12 doubles in the presence of magnetic fields. Though there is a larger difference for halo 12, the magnitude of the X-ray luminosity does not change significantly, suggesting that overall, the effects of magnetic fields might be small on the total X-ray luminosity, based on the simulated halos seen here. Nevertheless, due to the inconsistency in the measurement process of X-ray luminosity for each halo, it is hard to conclude the effects of magnetic fields since it is expected that most of the X-ray emission comes from the halo discs included in halos 12 and L8.

3.5.1 Comparing simulated X-ray luminosity with observations

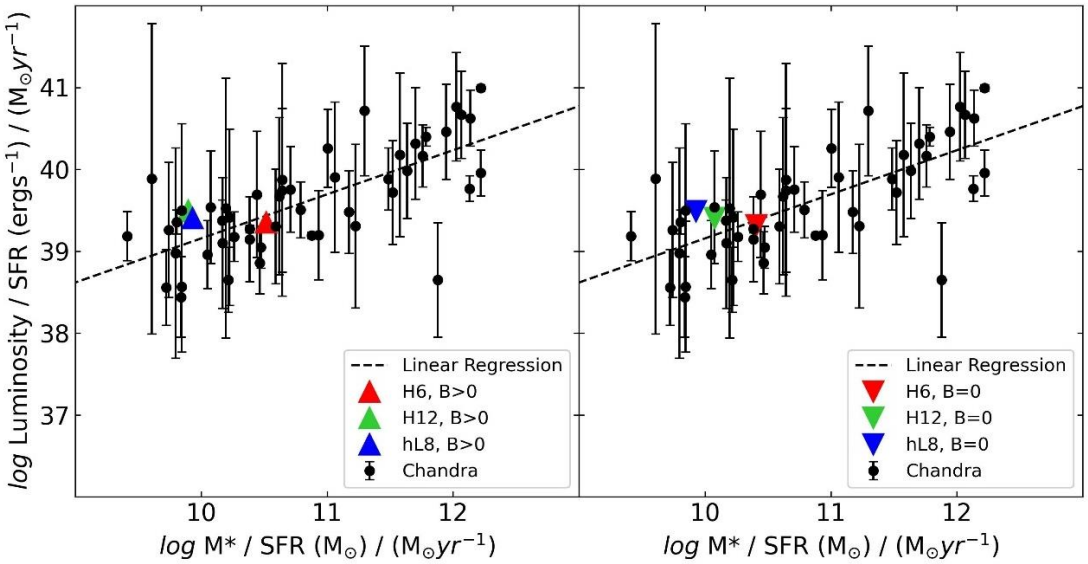

Figure 15: Lx/SFR (erg $s^{-1}/M_\odot yr^{-1}$) versus M*/SFR ($M_\odot/M_\odot yr^{-1}$) for observational and simulated halos. The black circles with error bars are observational data points from the Chandra survey analysed in Wang et al. 2016. The red, green, and blue triangles are the simulated halos, 6, 12 and L8 respectively. The black dashed line is a log-log linear regression "best-fit" line. The left-hand panel contains the simulated halos in the presence of magnetic fields. The right-hand panel contains the simulated halos in the absence of magnetic fields.

Figure 15 compares the total (0.5-2.0 keV) X-ray luminosity of the simulated halos, with observational galaxy halos with the relation Lx/SFR (erg $s^{-1}/M_\odot yr^{-1}$) versus M*/SFR ($M_\odot/M_\odot yr^{-1}$). Lx/SFR is found in the range 10^{37}-10^{42} (erg $s^{-1}/M_\odot yr^{-1}$). The uncertainty in the observational data is large. A Pearson correlation coefficient calculates a value of 0.69 for the observational data, suggesting a strong correlation. The simulated data halos 6, 12, and L8 are represented as the red, green, and blue triangles respectively. The left panel shows the simulated data in the presence of magnetic fields, the right panel shows the simulated data in the absence of magnetic fields. The simulated data seems to be consistent with the observational data and the best-fit line. A KS test value of 0.53 suggests that both data sets might be statistically similar. Furthermore, a p-value of 0.31 is found from the KS test, which is higher than the significance level of 0.05, suggesting that we can accept the null hypothesis that the two samples probably follow the same underlying distribution. The same KS values are found both in the presence and absence of magnetic fields suggesting that magnetic fields might have little to no effect on the total (0.5-2.0 keV) X-ray luminosity.

4.0 Discussion

The first key result found in this study is, is than in the presence of magnetic fields the CGM contains more hot gas ~10^6 K. Radial profiles for each simulated halo seen in figure 10, consistently show a higher gas temperature in the presence of magnetic fields within the CGM. The difference between the radial profiles in the presence and absence of magnetic fields is quantified by figure 11 which shows a median difference of 0.2 dex for all three simulated halos. Additionally, PDFs for temperature (figure 4), show a significant increase in probability of the gas reaching 10^6 K in the presence of magnetic fields. Furthermore, PDFs show a greater divide between the hot and cold gas in the CGM when magnetic fields are turned on, seen by a decrease in the probability of intermediate temperatures ~10^5 K. A possible reason for this effect is, as gas radiatively cools in the halo, it shock-heats the halo gas to the virial temperature, this brings about hot gas seen measured in this study. When the gas radiatively cools, it falls into smaller halo radii where it remains, likely supported by stronger magnetic fields found closer to the disc, i.e., where the magnetic pressure is greater than thermal pressure. Perhaps with the inclusion of an AGN feedback model, there might be an increase in the intermediate gas temperatures and the CGM might be cooler.

2D histograms (figure 13) provide further evidence for a warmer CGM in the presence of magnetic fields, since they show a greater amount of mass accumulating at the hot temperatures ~10^6 K. They also show a greater accumulation of cold gas in the halo discs. This is consistent with X-ray observations which suggest that the majority of baryonic matter resides in the discs but also within the halo gas in the form of virialized hot gas (Correa et al. 2018). The separation of hot and cold gas might be explained by the gas inflow/outflow velocity affecting the ability of the gas to mix. van de Voort et al. 2021 found that the presence of magnetic fields reduces the inflow and outflow velocities of gas. This leads to an enhancement of density in the centre of the halo, decreasing the temperature outside ~50 kpc, increasing the pressure, and so decreasing the amount of mixing in the CGM. This may also explain the lack of mixing seen by metals in the CGM.

The second key result found in this study is the small effect that magnetic fields have on the hydrogen number-density within the CGM. The small difference is evaluated in PDFs, radial profiles, and 2D histograms (figures 6, 10, & 13). Each showing a small decrease in hydrogen number-density of around 0.1 dex in the presence of magnetic fields within the CGM. The main effect magnetic fields have on the hydrogen density was actually on the halo discs which seem to retain more high-density gas than without. Therefore, the presence of magnetic fields decreases the hydrogen number-density in the CGM and increases within the halo discs, however, the difference is small. The reason magnetic fields have a small effect is not fully understood in this study.

The third key result in this study is that in the presence of magnetic fields the abundance of metals decreases by an average of 0.46 dex within the CGM. In-fact, in the presence of magnetic fields the metals seem to be contained mostly within the halo discs or in the hot gas ~ 10^6 K. This result is most notably seen in projections (figure 3) and 2D histograms (figure 13). But is most dramatically seen in radial profiles seen in figure 10, where metallicity is plotted in log and decreases roughly linearly with halo radius. Therefore, metallicity decreases exponentially with radius (measured from the central halo disc) when in the presence of magnetic fields. The CGM is therefore more metal rich in the absence of magnetic fields. Although, in both the presence and absence of magnetic fields, it is the halo discs that seem to retain much of the metal rich gas. This result might be explained by the decrease of inflow/outflow velocity in the presence of magnetic fields. In the absence of magnetic fields, metal rich gas retained inside the halo discs can escape (due to a lack of magnetic pressure)

and mix more easily with gas within the CGM. In the presence of magnetic fields the addition of further thermal pressure might promote mixing with more metal-rich gas, i.e., the inclusion of AGN in the simulations.

The examination of X-ray luminosity of simulated halos is on the forefront of new research. Figure 14 shows that all three simulated halos have a total 0.5-2.0 keV X-ray luminosity of the order 10^{40} erg s^{-1}. There is only a small difference in X-ray luminosity in the presence and absence of magnetic fields, especially in halo 6. However, in the case of halo 6, the X-ray luminosity was only calculated between 50-170 kpc to exclude the halo discs and therefore only measure emission from the CGM. The X-ray luminosity was measured from the disc centre out to 200 kpc for halos 12 and L8. It is then expected that the latter have a higher X-ray luminosity since the discs contain the hottest and most metal rich gas, where a majority of the X-ray emission is expected.

Figure 15 examines if the simulated luminosity is consistent with observational data and the power laws analysed by (Wang et al. 2016). It is found that both simulated X-ray luminosity (in the presence and absence of magnetic fields) is consistent with the power law plotted in figure 15 of Lx/SFR versus M*/SFR. Both data sets have a KS test value of 0.53 and a p-value of 0.31 suggesting that both data sets are probably from the same underlying distribution and are a match. This consistency in the data was not found for Lx versus M*, (appendix, figure 12) probably due to a low Pearson correlation coefficient.

Further study should be examined to test if the simulated halos match other observational data sets and relations. More importantly, their consistency with the data should be examined with more realistic simulation conditions, including all feedback mechanisms such as AGN. Additionally, X-ray luminosity for Halo 12 and Halo L8 should be measured by excluding their halo discs in order to only measure emission from the CGM. Furthermore, the variation of metallicity per cell was not considered in the calculations for X-ray luminosity. Instead it was assumed that every cell had a metallicity equal to the solar abundance of metals.

5.0 Conclusions

This study shows that magnetic fields have an effect on the temperature, hydrogen number-density, and metallicity of the gaseous component of simulated halos. It is found that in the presence of magnetic fields, the CGM temperature is warmer by ~0.2 dex reaching temperatures closer to ~10^6 K and creates a greater divide in the cold and hot gas temperatures i.e., a decrease in the intermediate temperatures ~10^5 K. The presence of magnetic fields has the greatest effect on the CGM metallicity with an average decrease of ~0.46 dex. So, in the presence of magnetic fields, the CGM is less metal-rich. These two effects might be explained by the decrease in the inflow/outflow velocities in the presence of magnetic fields, reducing the ability for gas to mix. The hydrogen number-density decreases only by a small amount, at around ~0.1 dex, and so the presence of magnetic fields have a small effect on the hydrogen number-density in the CGM. However, the reason for the low impact of magnetic fields on the hydrogen number-density is not explained in this study.

This study measures the total 0.5-2.0 keV X-ray luminosity for halos 6, 12, and L8 and finds luminosities of the order 10^{40} erg s^{-1}. These results are consistent with observational data of 52 star-forming galaxies and their linear log-log relation of Lx/SFR versus M*/SFR, analysed in Wang et al. 2016. It is found that magnetic fields might have little to no effect on the X-ray luminosity. However, due to the lack of consistency in the measurements of X-ray emission from the simulated halos, further work should follow to investigate the effects of magnetic fields.

6.0 Bibliography

Biermann, L. 1951. Cosmic Radiation and Cosmic Magnetic Fields. II. Origin of Cosmic Magnetic Fields. *Physical Review* 82(6), pp. 863–868. doi: 10.1103/PhysRev.82.863.

Chadayammuri, U., Bogdan, A., Oppenheimer, B., Kraft, R., Forman, W. and Jones, C. 2022. Testing galaxy feedback models with the first resolved profiles of the circumgalactic medium. *arXiv:2203.01356 [astro-ph]* . Available at: http://arxiv.org/abs/2203.01356 [Accessed: 5 April 2022].

Chen, H.-W., Lanzetta, K.M., Webb, J.K. and Barcons, X. 1998. The Gaseous Extent of Galaxies and the Origin of Lyα Absorption Systems. III. 1. *The Astrophysical Journal* 498(1), pp. 77–94. doi: 10.1086/305554.

Choudhury, P.P., Sharma, P. and Quataert, E. 2019. Multiphase gas in the circumgalactic medium: relative role of tcool/tff and density fluctuations. *Monthly Notices of the Royal Astronomical Society* 488, pp. 3195–3210. doi: 10.1093/mnras/stz1857.

Correa, C.A., Schaye, J., Wyithe, J.S.B., Duffy, A.R., Theuns, T., Crain, R.A. and Bower, R.G. 2018. The formation of hot gaseous halos around galaxies. *Monthly Notices of the Royal Astronomical Society* 473(1), pp. 538–559. doi: 10.1093/mnras/stx2332.

Das, S., Mathur, S., Nicastro, F. and Krongold, Y. 2019. Discovery of a Very Hot Phase of the Milky Way Circumgalactic Medium with Non-solar Abundance Ratios. *The Astrophysical Journal* 882(2), p. L23. doi: 10.3847/2041-8213/ab3b09.

Dolag, K., Bartelmann, M. and Lesch, H. 1999. SPH simulations of magnetic fields in galaxy clusters. *arXiv:astro-ph/9906329* . Available at: http://arxiv.org/abs/astro-ph/9906329 [Accessed: 30 April 2022].

Dubois, Y. and Teyssier, R. 2008. Cosmological MHD simulation of a cooling flow cluster. *Astronomy & Astrophysics* 482(2), pp. L13–L16. doi: 10.1051/0004-6361:200809513.

Giacalone, J. 2013. Cosmic-Ray Transport and Interaction with Shocks. *Space Science Reviews* 176(1–4), pp. 73–88. doi: 10.1007/s11214-011-9763-2.

Gómez, F.A., White, S.D.M., Grand, R.J.J., Marinacci, F., Springel, V. and Pakmor, R. 2017. Warps and waves in the stellar discs of the Auriga cosmological simulations. *Monthly Notices of the Royal Astronomical Society* 465, pp. 3446–3460. doi: 10.1093/mnras/stw2957.

Grand, R.J.J. et al. 2017. The Auriga Project: the properties and formation mechanisms of disc galaxies across cosmic time. *Monthly Notices of the Royal Astronomical Society* 467(1), pp. 179–207. doi: 10.1093/mnras/stx071.

Grand, R.J.J. et al. 2019. Gas accretion and galactic fountain flows in the Auriga cosmological simulations: angular momentum and metal redistribution. *Monthly Notices of the Royal Astronomical Society* 490(4), pp. 4786–4803. doi: 10.1093/mnras/stz2928.

Grand, R.J.J., Springel, V., Gómez, F.A., Marinacci, F., Pakmor, R., Campbell, D.J.R. and Jenkins, A. 2016. Vertical disc heating in Milky Way-sized galaxies in a cosmological context. *Monthly Notices of the Royal Astronomical Society* 459, pp. 199–219. doi: 10.1093/mnras/stw601.

Han, J.L. 2017. Observing Interstellar and Intergalactic Magnetic Fields. *Annual Review of Astronomy and Astrophysics* 55(1), pp. 111–157. doi: 10.1146/annurev-astro-091916-055221.

Haverkorn, M. and Heesen, V. 2012. Magnetic Fields in Galactic Haloes. *Space Science Reviews* 166, pp. 133–144. doi: 10.1007/s11214-011-9757-0.

Kelly, A.J., Jenkins, A. and Frenk, C.S. 2021. The origin of X-ray coronae around simulated disc galaxies. *Monthly Notices of the Royal Astronomical Society* 502(2), pp. 2934–2951. doi: 10.1093/mnras/stab255.

Lanzetta, K.M., Bowen, D.V., Tytler, D. and Webb, J.K. 1995. The Gaseous Extent of Galaxies and the Origin of Lyman-Alpha Absorption Systems: A Survey of Galaxies in the Fields of Hubble Space Telescope Spectroscopic Target QSOs. *The Astrophysical Journal* 442, p. 538. doi: 10.1086/175459.

Li, J.-T., Crain, R.A. and Wang, Q.D. 2014. Chandra survey of nearby highly inclined disc galaxies - III. Comparison with hydrodynamical simulations of circumgalactic coronae. *Monthly Notices of the Royal Astronomical Society* 440, pp. 859–869. doi: 10.1093/mnras/stu329.

Li, J.-T. and Wang, Q.D. 2013a. Chandra survey of nearby highly inclined disc galaxies – I. X-ray measurements of galactic coronae. *Monthly Notices of the Royal Astronomical Society* 428(3), pp. 2085–2108. doi: 10.1093/mnras/sts183.

Li, J.-T. and Wang, Q.D. 2013b. Chandra survey of nearby highly inclined disc galaxies - II. Correlation analysis of galactic coronal properties. *Monthly Notices of the Royal Astronomical Society* 435, pp. 3071–3084. doi: 10.1093/mnras/stt1501.

Marinacci, F., Grand, R.J.J., Pakmor, R., Springel, V., Gómez, F.A., Frenk, C.S. and White, S.D.M. 2017. Properties of H I discs in the Auriga cosmological simulations. *Monthly Notices of the Royal Astronomical Society* 466, pp. 3859–3875. doi: 10.1093/mnras/stw3366.

Marinacci, F., Vogelsberger, M., Mocz, P. and Pakmor, R. 2015. The large-scale properties of simulated cosmological magnetic fields. *arXiv:1506.00005 [astro-ph]* . Available at: http://arxiv.org/abs/1506.00005 [Accessed: 28 April 2022].

Monachesi, A. et al. 2019. The Auriga stellar haloes: connecting stellar population properties with accretion and merging history. *Monthly Notices of the Royal Astronomical Society* 485, pp. 2589–2616. doi: 10.1093/mnras/stz538.

Pakmor, R. et al. 2017. Magnetic field formation in the Milky Way like disc galaxies of the Auriga project. *Monthly Notices of the Royal Astronomical Society* 469, pp. 3185–3199. doi: 10.1093/mnras/stx1074.

Pakmor, R. and Springel, V. 2013. Simulations of magnetic fields in isolated disk galaxies. *Monthly Notices of the Royal Astronomical Society* 432(1), pp. 176–193. doi: 10.1093/mnras/stt428.

Simpson, C.M. et al. 2018. Quenching and ram pressure stripping of simulated Milky Way satellite galaxies. *Monthly Notices of the Royal Astronomical Society* 478, pp. 548–567. doi: 10.1093/mnras/sty774.

Spitzer, L., Jr. 1956. On a Possible Interstellar Galactic Corona. *The Astrophysical Journal* 124, p. 20. doi: 10.1086/146200.

Springel, V. 2010a. Moving-mesh hydrodynamics with the AREPO code. *Proceedings of the International Astronomical Union* 6(S270), pp. 203–206. doi: 10.1017/S1743921311000378.

Springel, V. 2010b. Smoothed Particle Hydrodynamics in Astrophysics. *Annual Review of Astronomy and Astrophysics* 48(1), pp. 391–430. doi: 10.1146/annurev-astro-081309-130914.

Springel, V., White, S.D.M., Tormen, G. and Kauffmann, G. 2001. Populating a cluster of galaxies – I. Results at z ¼ 0., p. 25.

Stinson, G.S. et al. 2012. MAGICC haloes: confronting simulations with observations of the circumgalactic medium at z = 0. *Monthly Notices of the Royal Astronomical Society* 425(2), pp. 1270–1277. doi: 10.1111/j.1365-2966.2012.21522.x.

Tumlinson, J. et al. 2011. The Large, Oxygen-Rich Halos of Star-Forming Galaxies Are a Major Reservoir of Galactic Metals. *Science* 334, p. 948. doi: 10.1126/science.1209840.

Tumlinson, J., Peeples, M.S. and Werk, J.K. 2017. The Circumgalactic Medium. *Annual Review of Astronomy and Astrophysics* 55(1), pp. 389–432. doi: 10.1146/annurev-astro-091916-055240.

van de Voort, F. et al. 2016. The impact of stellar feedback on hot gas in galaxy haloes: the Sunyaev-Zel'dovich effect and soft X-ray emission. *Monthly Notices of the Royal Astronomical Society* 463, pp. 4533–4544. doi: 10.1093/mnras/stw2322.

van de Voort, F., Bieri, R., Pakmor, R., Gómez, F.A., Grand, R.J.J. and Marinacci, F. 2021. The effect of magnetic fields on properties of the circumgalactic medium. *Monthly Notices of the Royal Astronomical Society* 501(4), pp. 4888–4902. doi: 10.1093/mnras/staa3938.

Wang, Q.D., Li, J., Jiang, X. and Fang, T. 2016. Chandra survey of nearby highly inclined disk galaxies - IV. New insights into the working of stellar feedback. *Monthly Notices of the Royal Astronomical Society* 457, pp. 1385–1392. doi: 10.1093/mnras/stv2886.

Wechsler, R.H. and Tinker, J.L. 2018. The Connection Between Galaxies and Their Dark Matter Halos. *Annual Review of Astronomy and Astrophysics* 56(1), pp. 435–487. doi: 10.1146/annurev-astro-081817-051756.

White, S.D.M. and Rees, M.J. 1978. Core condensation in heavy halos: a two-stage theory for galaxy formation and clustering. *Monthly Notices of the Royal Astronomical Society* 183(3), pp. 341–358. doi: 10.1093/mnras/183.3.341.

Widrow, L.M., Ryu, D., Schleicher, D.R.G., Subramanian, K., Tsagas, C.G. and Treumann, R.A. 2012. The First Magnetic Fields. *Space Science Reviews* 166, pp. 37–70. doi: 10.1007/s11214-011-9833-5.

Wijers, N.A. and Schaye, J. 2021. The warm-hot circumgalactic medium around EAGLE-simulation galaxies and its detection prospects with X-ray line emission. *arXiv:2108.04847 [astro-ph]* . Available at: http://arxiv.org/abs/2108.04847 [Accessed: 13 October 2021].